IEEE Access
Multidisciplinary | Rapid Review | Open Access Journal

Received December 21, 2019, accepted January 3, 2020, date of publication January 7, 2020, date of current version February 6, 2020.

Digital Object Identifier 10.1109/ACCESS.2020.2964721

Patch Antenna Loaded With Paired Shorting Pins and H-Shaped Slot for 28/38 GHz Dual-Band MIMO Applications

PENGFEI LIU, (Student Member, IEEE), XIAO-WEI ZHU, (Member, IEEE), YAN ZHANG, (Member, IEEE), XIANG WANG, (Student Member, IEEE), CHUNFENG YANG, AND ZHI HAO JIANG, (Member, IEEE)

State Key Laboratory of Millimeter Waves, Southeast University, Nanjing 210096, China

Corresponding author: Xiao-Wei Zhu (xwzhu@seu.edu.cn)

This work was supported in part by the National Natural Science Foundation of China under Grant 61861136002 and Grant 61671149.

ABSTRACT A novel dual-band patch antenna operating at 28/38 GHz is proposed for multiple-input multiple-output (MIMO) communication systems in this paper. The antenna utilizes substrate integrated waveguide (SIW) transmission line as the feed by means of a coupling slot on the SIW. A square patch antenna functions as the radiator for 28 GHz. The inductive loading, which presents as a pair of shorting pins in this design, achieves the impedance matching for 28 GHz-band. Etched on the square patch, the proposed H-shaped slot makes the radiator to performance as an antenna containing two radiating arms and thus introduces another resonant frequency at 38 GHz. Directions of the surface current on the paired arms are identical and produce a reasonable radiation pattern for 38 GH-band. Simulated results declare that the antenna achieves an $S_{11} < -10$ dB bandwidth of 27.6 – 28.5 GHz (relative bandwidth of 3.2%) and 36.9 – 38.9 GHz (relative bandwidth of 5.3%), while simulated gain is 9.0 dBi at 28 GHz and 5.9 dBi at 38 GHz, respectively. Measured results have verified the feasibility and correctness of the proposed dual-band antenna, which indicate that the antenna is a promising candidate for MIMO communication systems at millimeter-wave (mmW) band.

INDEX TERMS Dual-band, patch antenna, 28/38 GHz, multiple-input multiple-output (MIMO), shorting pin, H-shaped slot, millimeter-wave (mmW).

I. INTRODUCTION

Nowadays, the fifth generation (5G) has already entered the formal commercial stage since the associated infrastructure constructions along with the terminal installations are increasingly researched and improved [1]. At present, lower frequencies (sub-6 GHz) which are utilized for wide area coverage are already in use for the 5G technique, while the higher frequencies, *i.e.* millimeter-wave (mmW) bands, for local area networks and short-range indoor links are still in developing [2]–[7]. Compared with the sub-6 GHz band, the upcoming usage of mmW band will undoubtedly further advance the efficient communication experience because of its broad bands and thus the capability of delivering multi-gigabit per second data speeds [8]–[12]. To establish their own standardization as quickly as possible, a lot of countries have identified their frequencies for 5G mmW applications, such as 27.5-28.8 GHz for Japan, 28 GHz for Korea and 24.25-27.5 GHz/37-43.5 GHz for China [13]–[16]. For the United States, as early as October 2015, Federal Communications Commission (FCC) has recommended that the spectrum around 28 GHz, 37 GHz, 39 GHz and 64-71 GHz should be under strong consideration. Hence, devices for these bands are of particular importance for 5G communication systems [17], [18].

As a significant solution for 5G applications, antennas with multiple bands property are applicable owing to their capabilities to keep the devices compact in size [19]–[24]. On the contrary, complex feed networks for multiple independent antennas will produce the additional loss, which could be a clear disadvantage especially for mmW bands. Hence, multi-band antennas have been research focuses in the field of

The associate editor coordinating the review of this manuscript and approving it for publication was Guan Gui.

mmW antennas. For the realization of dual-band antennas, an often-adopted design method is gathering two radiating elements together with some techniques. The method applies whether or not is determined by the structures of the single frequency antennas. Another way is utilizing a single element which can working at two segregate modes. However, the shortcoming of the latter approach is that the operating frequencies of most antennas cannot be easily adjusted separately.

In this paper, a novel dual-band patch antenna, which is intended for operation at 28 GHz and 38 GHz bands, is proposed for the forthcoming 5G mmW applications. A narrow slot on a substrate integrated waveguide (SIW) transmission line couples the electromagnetic energies to the radiating patch, while the upper metal layer of the SIW also functions as the ground of the patch at the same time. Two metallized shorting pins inductively load on the patch antenna, and thus generate a resonant frequency at 28 GHz. With the operating band at 28 GHz maintained, an H-shaped slot is etched on the patch antenna and introduces another working mode at 38 GHz.

This article has been divided into five parts. Section II gives an overview of the proposed dual-band patch antenna. Section III discusses the operating principle at the dual-band frequencies respectively while section IV presents a detailed analysis of the antenna. In section V, this paper focuses on the measured results and studies the reasons which could cause the discrepancies between measurement and simulation. In the end of this work, a conclusion is drawn in Section VI.

II. CONFIGURATION OF THE DUAL-BAND ANTENNA

Fig. 1 depicts the configuration of proposed dual-band antenna. The antenna is constructed by a stack of two dielectric layers and three metallization layers. Both of the two dielectric layers (Substrate #1 and Substrate #2 in Fig. 1) are composed of Taconic TLY-5 with a relative permittivity (ε_r) of 2.2 and a dielectric loss tangent (tan δ) of 0.0009. Put slightly differently, the upper Substrate #1 is in a thickness of $h_1 = 0.508$ mm while the lower Substrate #2 has a thickness of $h_2 = 0.254$ mm. On the Substrate #2 board, a microstrip-to-SIW transition, which transfers energy form connector to SIW transmission line, is etched. A transverse slot is grooved on the SIW structure to excite the radiating patch which is bonded on Substrate #1 board. At both sides of the transverse slot, there exists a pair of metallized shorting pins connecting the radiating patch to the upper metallization layer of the SIW transmission line. On the top layer, a special H-shaped slot with optimized dimensions is etched on the patch. The geometries of the two slabs and the three metallization layers on them are shown in Fig. 2, while the detailed dimensions of the proposed antenna are given in Table 1.

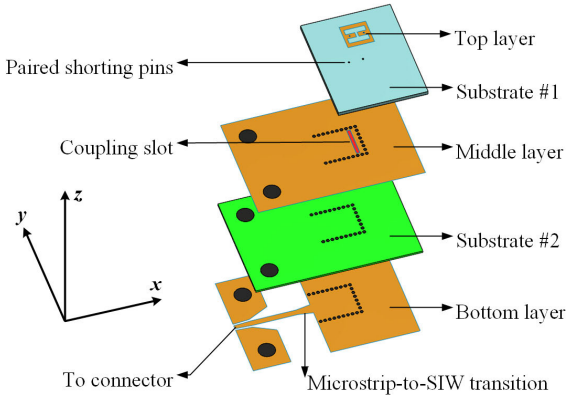

FIGURE 1. Configuration of proposed dual-band antenna.

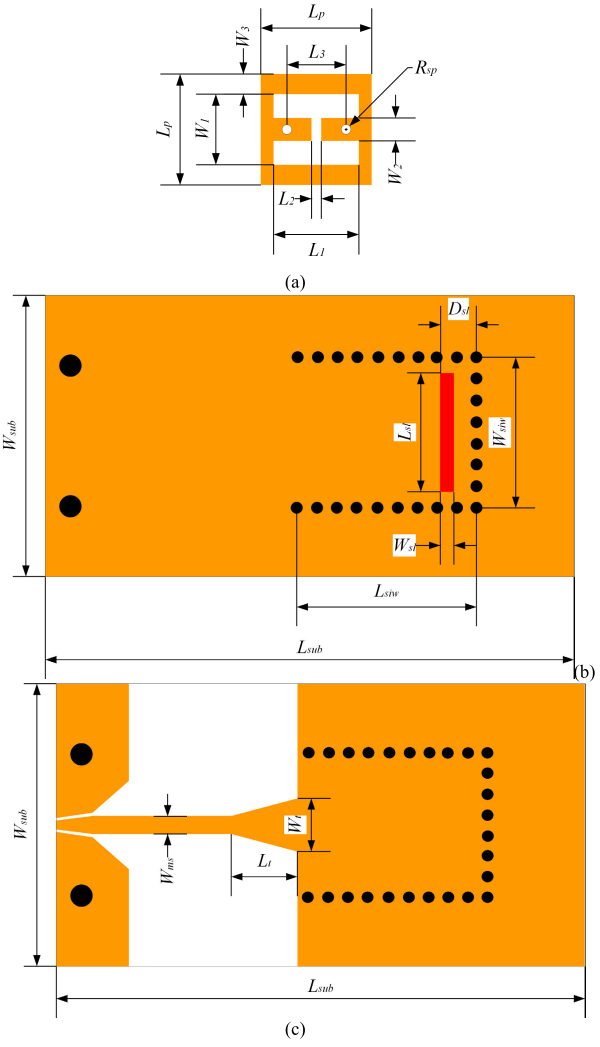

FIGURE 2. Geometries of the three metallization layers. (a) top layer, (b) middle layer, (c) bottom layer.

III. OPERATING PRINCIPLE AND EVOLUTION OF THE DUAL-BAND ANTENNA

A. INDEPENDENT ANTENNA WORKING AT 28 GHz

This paper utilizes a reported method for the lower operating frequency of 28 GHz, *i.e.* a pair of shorting pins for inductive loading [25]. Diameter of the paired shorting pins in Fig. 3(a)

TABLE 1. Dimension of the proposed dual-band antenna in Fig. 2 (units: mm).

Parameter	L_1	L_2	L_3	W_1	W_2	W_3	L_p
Value	2.71	0.306	1.85	2.23	0.73	0.625	3.48
Parameter	R_{sp}	L_{sl}	W_{sl}	D_{sl}	L_{siw}	W_{siw}	L_{sub}
Value	0.1	3.9	0.445	1.222	5.4	4.62	25
Parameter	W_{sub}	L_t	W_t	W_{ms}			
Value	15	1.975	1.4	0.78			

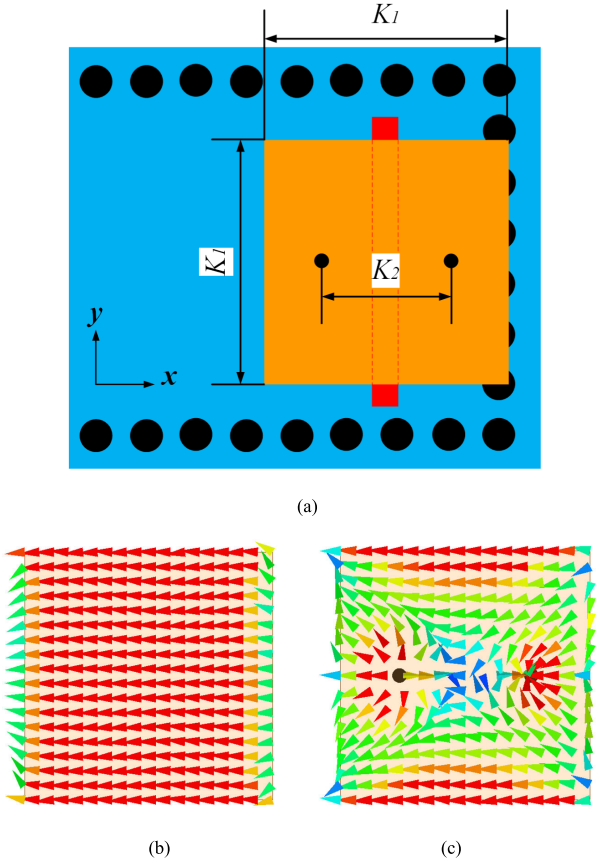

FIGURE 3. (a) Configuration of the 28 GHz-band patch antenna loaded with paired shorting pins, (b) surface current of patch antenna without paired shorting pins, (c) surface current of patch antenna with paired shorting pins.

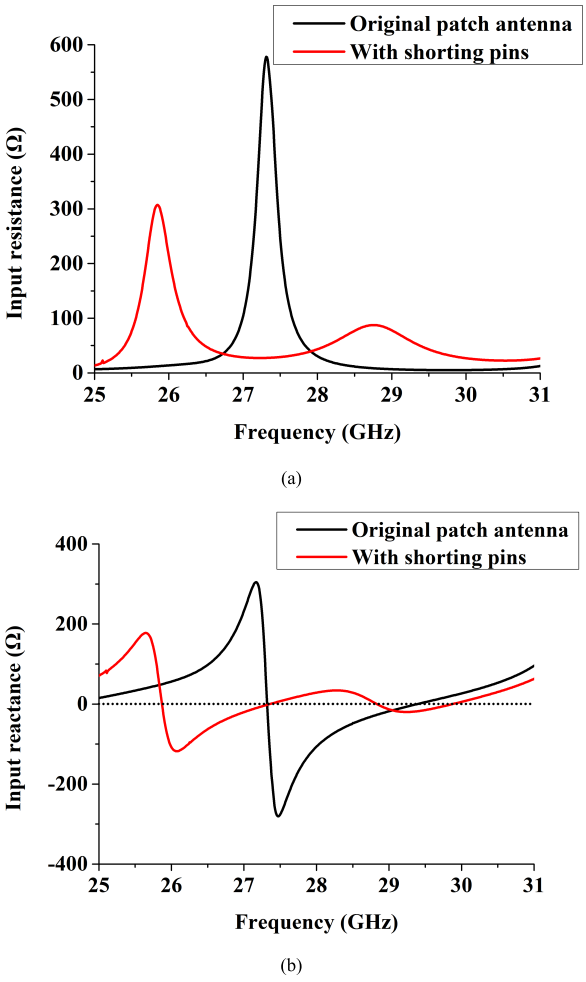

FIGURE 4. Input resistance (R_{in}) and reactance (X_{in}) of the patch antennas. (a) input resistance (R_{in}), (b) input reactance (X_{in}).

is 0.2 mm while distance between the pins is $K_2 = 1.85$ mm and the patch length is $K_1 = 3.48$ mm. The current distributions of the patch without and with paired shorting pins are also illustrated in Fig. 3(b) and (c). According to surface current distributions, the paired shorting pins, which functions as the inductive loading for the patch antenna, make the surface currents concentrate at the two edges in the y direction of the patch and the region nearby the paired pins. Moreover, in Fig. 3(b), the currents around the shorting pins contribute little to the radiation patterns for 28 GHz. At the operating frequency around 28 GHz-band, the input resistance (R_{in}) and reactance (X_{in}) of the patch antenna without and with the shorting pins are shown in Fig. 4. For the original patch antenna, simulated R_{in} at 28 GHz is 29 Ω while X_{in} is −107 Ω, which signifies a high capacitive input impedance characteristic. According to the analysis in [25], paired shorting pins along the centerline could bring in significant shunt-inductive effect to the patch antenna. In our design, with the paired-shorting-pins loaded, the input X_{in} at 28 GHz is increased to approximate 28 Ω.

B. INDEPENDENT ANTENNA WORKING AT 38 GHz

For the 38 GHz-band, Fig. 5(a) shows a novel antenna which also utilizes a coupling slot on the SIW transmission line for feeding just as the previously mentioned patch antenna working at 28 GHz (see Fig. 3). Main radiation source of the 38 GHz-band antenna is a pair of arms while two shorting pins connect the arms to the upper layer of the SIW transmission line, respectively. The sufficiently large upper layer functions as the ground of the antenna operating at 38 GHz. As Fig. 5(b) shows, surface currents at 38 GHz are concentrated in the nearby regions of shorting pins. The amplitude of the surface currents between the shorting pins is much higher than the value of currents outside the paired shorting pins. And amplitude of the current is minimal at the end of the arms. Meanwhile, directions of the surface currents on the arms are accordant at the same time, which indicate the two identical

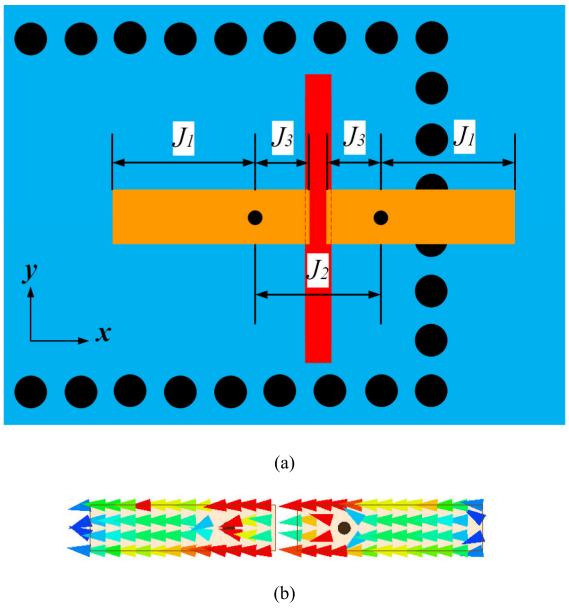

FIGURE 5. (a) Configuration of the 38 GHz-band antenna, (b) surface current on the radiating arms of the 38 GHz-band antenna.

currents will generate a superimposed radiation in the far field at 38 GHz.

According to the surface current on the arms, the length J_1, J_2 and J_3 in Fig. 5(a) are main influencing factors for the resonance of the 38 GHz-band antenna. Fig. 6 illustrates the simulated reflection coefficient for variations on J_1, J_2, J_3 and clears that the increases of J_1, J_2, J_3 will cause band shifts towards lower frequencies. Hence, all of the lengths J_1, J_2 and J_3 can be used for band tuning for 38 GHz-band antenna.

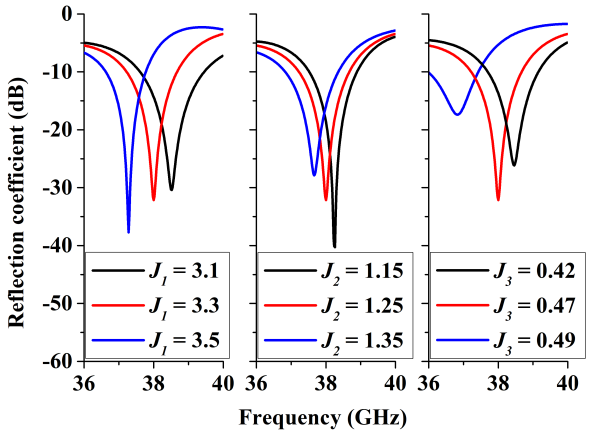

FIGURE 6. Simulated reflection coefficient of the 38 GHz-band antenna in Fig. 5(a) for variations on J_1, J_2 and J_3 (Unit of J_1, J_2 and J_3: mm).

C. EVOLUTION OF THE DUAL-BAND ANTENNA

This paper proposed a novel dual-band antenna which combines the 28 GHz-band and 38 GHz-band antennas together. The final design of the radiating patch is presented in Fig. 7(a), while Fig. 7(b) and (c) show the surface current distributions on the patch at 28 and 38 GHz respectively.

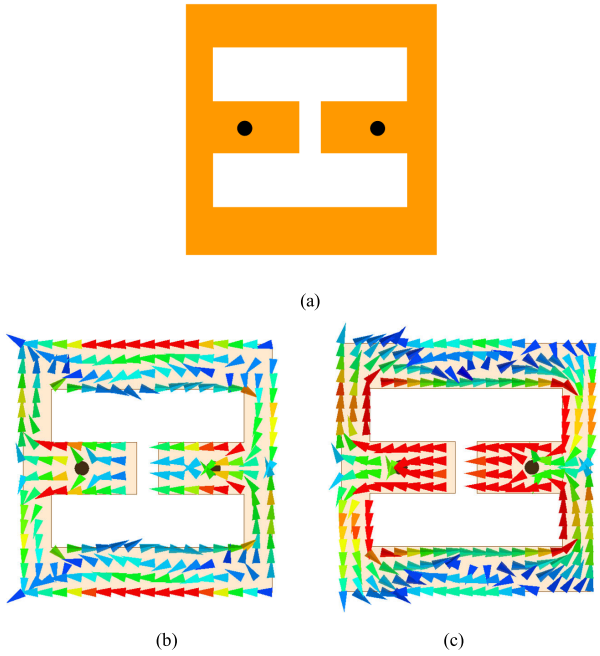

FIGURE 7. (a) Final design of the patch antenna for dual-band, (b) surface current distribution on the final designed patch at 28 GHz, (b) surface current distribution on the final designed patch at 38 GHz.

On the basis of current distributions of the dual-band antenna, compared with the surface current described as Fig. 3(c), the main radiating region of the 28 GHz-band antenna, which locates at the edges of the patch, remains unchanged. The etched H-shaped slot removes the metallic part passing through with minor currents. In the respect of impedance characteristic, the input resistance will not varies dramatically when the H-shaped slot etched on the patch, while the input reactance (X_{in}) at 28 GHz will decrease from 28 Ω to 6.7 Ω. In fact, the added H-shaped slot has just a little capacitive loading effect for the patch antenna on the operating band of 28 GHz.

At 38 GHz, each end of the two radiating arms in Fig. 5 is separated and arranged in y direction. On the basis of surface current distribution on the final designed patch at 38 GHz, connection of the two radiating arms has almost no influence on the current distribution around the paired shorting pins. And the region which contributes a lot for radiating is preserved. For the far field performance, the currents (see Fig. 7(c)) in the y direction are toward opposite directions and thus cancel each other out for radiation.

In addition, the simulated radiation patterns of the dual-band antenna at 28 and 38 GHz are presented in Fig. 8. Since the both of the surface current directions at 28 and 38 GHz are in the x axis, predominant polarization directions at the two frequency mode are identical with each other.

IV. ANALYSIS OF THE DUAL-BAND ANTENNA

Fig. 9 depicts the simulated reflection coefficient for variations on the patch length L_p. According to Fig. 9, the length L_p decides the lower resonant frequency while it has little

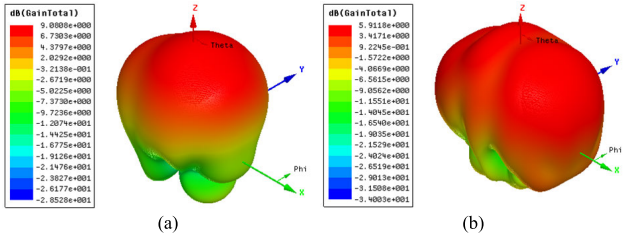

FIGURE 8. Simulated far field radiation patterns of the dual-band antenna, (a) 28 GHz, (b) 38 GHz.

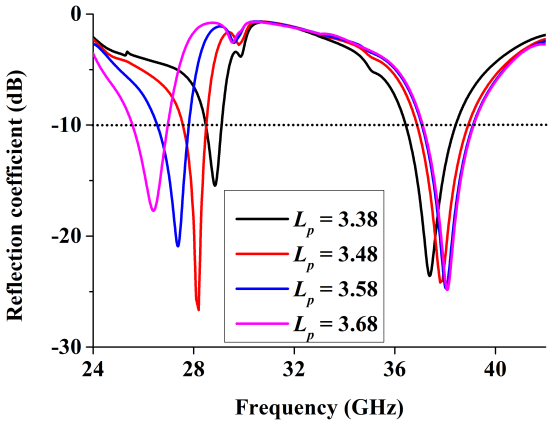

FIGURE 9. Simulated reflection coefficient for variations on the patch length L_p(Unit of L_p: mm).

influence on the higher resonant frequency. There is no doubt that increasing the length of the patch will lead to a shift for 28 GHz band towards lower frequencies since the surface current path at the edge of the patch is lengthened. And on the other hand, a small increase of L_p mainly maintains the impedance characteristics for the antenna working at 38 GHz. A slight band shift to lower frequency occurs at 38 GHz band while L_p is reduced from 3.68 mm to 3.38 mm. This is because the length L_p has an effect on the currents in the y direction and thus a slight change is carried out for the resonant frequency of the independent 38 GHz-band antenna. Therefore, to a certain extent, independent tuning in 28 and 38 GHz band can be realized by L_p.

An analogous situation occurs on the dimension parameter of L_2, which represents the dimension of the gap between the paired radiating arms in Fig 5. In the region nearby the gap, surface current amplitudes at 28 GHz are minimal on the basis of Fig. 7(c). Hence, the variations on L_2 will not basically affect the impedance matching for 28 GHz band. For 38 GHz band, the gap between paired arms determines the arm lengths of the antenna working at 38 GHz and thus determines the resonant frequency for the higher band. When the length of the gap (L_2) is increased, arms of the antenna for 38 GHz are longer, which corresponds a shift to lower frequencies. Simulated reflection coefficient for variations on the gap distance L_2 is presented in Fig. 10. In accordance with Fig. 10, resonances in the 28 GHz band remain unaffected while L_2 varies from 0.206 mm to 0.406 mm. And the bandwidth of the higher operating band does not decrease for variations on L_2.

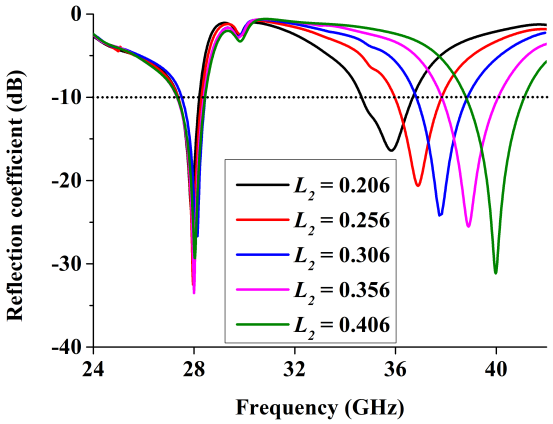

FIGURE 10. Simulated reflection coefficient for variations on the gap distance L_2(Unit of L_2: mm).

Consequently, Fig. 10 proves the analysis above and indicates that except for L_p, the gap length L_2 can be applied for another independent tuning of the proposed dual-band antenna.

Obviously, parameters which determine the level of inductive loading of the antenna working at 28 GHz and the arm length of the antenna working at 38 GHz will define the both resonances of the dual-band antenna. Fig. 11 depicts the simulated reflection coefficient for variations on paired shorting pins distance L_3. A significant tendency in Fig. 11 is that the frequency difference between the two resonances comes closer while L_3 is increasing. This phenomenon can be explained as follows. For 28 GHz band, increase of L_3 makes the pins approaching to the edges (in the x axis direction) of the patch and thus the shunt-inductive effect b–rought in by pins pushes up the resonant frequency. For 38 GHz band, increase of L_3 enables a longer arm length of the antenna operating at 38 GHz, which pulls down the resonant frequency for the higher band of proposed antenna.

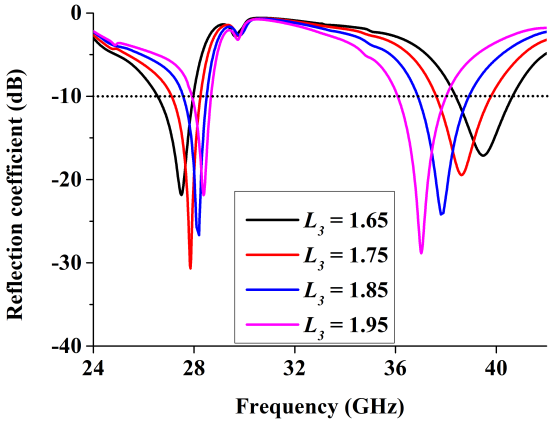

FIGURE 11. Simulated reflection coefficient for variations on the paired shorting pins distance L_3(Unit of L_3: mm).

Similar results are obtained for the parameter R_{sp}which represents the radii of the paired shoring pins. Fig. 12 claims that with the pin radii of R_{sp} = 0.1 mm increasing to R_{sp} = 0.15 mm and 0.2 mm, the lower resonant of the

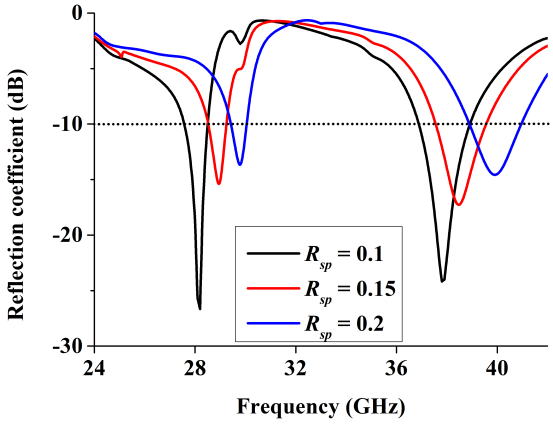

FIGURE 12. Simulated reflection coefficient for variations on the radii of paired shorting pins R_{sp}(Unit of R_{sp}: mm).

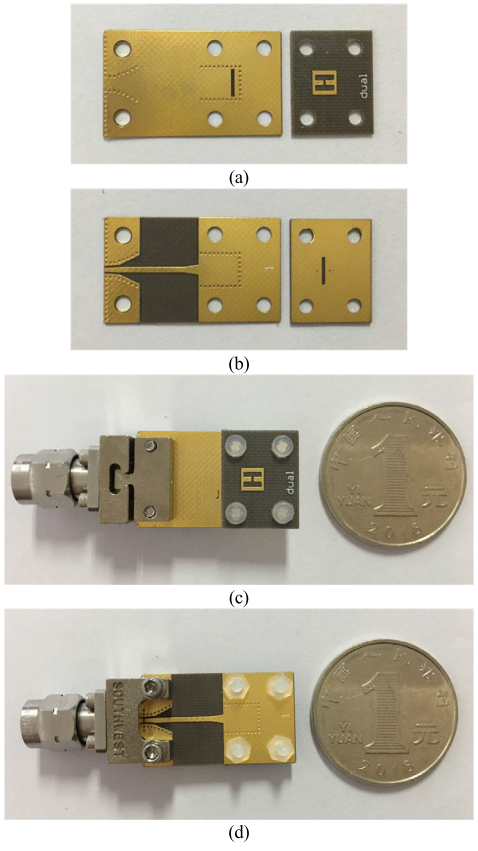

FIGURE 13. Photographs of the dual-band antenna prototype. (a) top view of Substrate #1 and Substrate #2, (b) bottom view of Substrate #1 and Substrate #2, (c) top view of the proposed antenna with connector, (d) bottom view of the proposed antenna with connector.

dual-band antenna will move towards the higher band. For the 38 GHz-band, a bigger pin radii means a shorter arm length is used for radiating, which produces a higher operating frequency for the upper band of the dual-band antenna. Hence, the two working bands have the coincident tendency upon the pin radii R_{sp}.

V. MEASURED RESULTS

Fig. 13 shows prototypes of the separated slabs marked as Substrate #1 and Substrate #2 described in Fig. 1, as well as the photos of fabricated entire dual-band antenna. Proposed antenna is fed by a 2.40mm Southwest End Launcher and is measured with a vector network analyzer (Keysight N5247A). The simulated and measured reflection coefficients of the dual-band antenna are depicted in Fig. 14. As the figure shown, the fabricated antenna covers two separated $S_{11} < -10$ dB band ranges of 27.7-28.7 GHz and 36.8-40.2 GHz, which are broader than the simulated

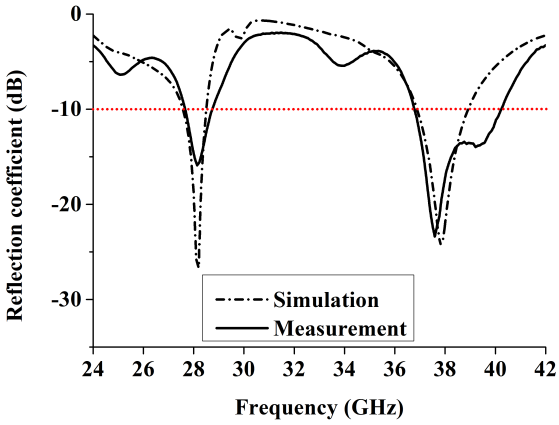

FIGURE 14. Simulated and measured reflection coefficients of the proposed dual-band antenna.

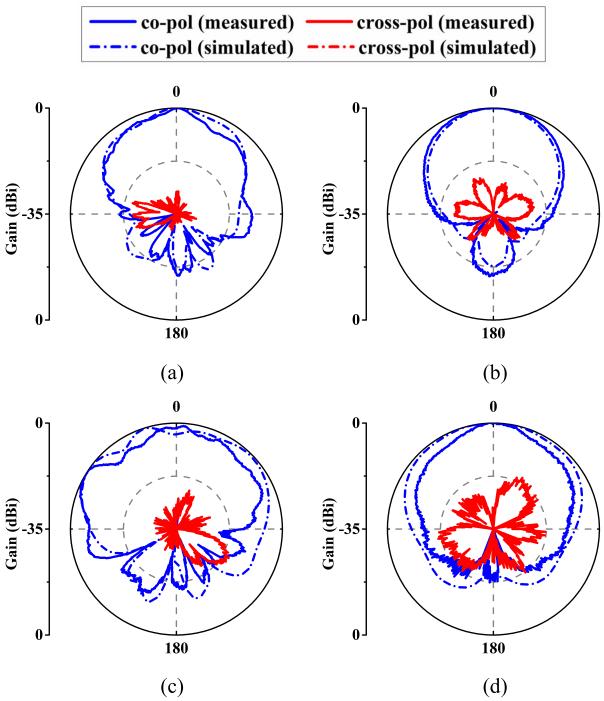

FIGURE 15. Simulated and measured normalized radiation patterns of the proposed dual-band antenna, (a) E-plane at 28 GHz, (b) H-plane at 28 GHz, (c) E-plane at 38 GHz, (d) H-plane at 38 GHz.

values of 27.6-28.5 GHz and 36.9-38.9 GHz. Discrepancies between simulation and measurement can be attribute to the fabrication and assembly inaccuracy of the antenna, while transmission loss of Southwest End Launcher aggravates the discrepancies.

The proposed dual-band antenna is measured in anechoic chamber and the normalized radiation patterns at 28 and 38 GHz are displayed in Fig. 15. According to Fig. 15, for both of the two operating frequencies, measured co-polarized patterns differ slightly from the simulation while the deviations are caused by assembly error of the antenna and reflection effect of the metallic connector. In both E- and H-planes, normalized cross-polarizations by measurement are below −16.0 dB. Moreover, measured gains of the proposed dual-band antenna are 8.4 dBi at 28 GHz and 6.1 dBi at 38 GHz while the radiating efficiencies at the two operation bands are 84% and 99%, respectively.

VI. CONCLUSION

A dual-band patch antenna working at 28/38 GHz is proposed manufactured, and validated in this paper. To feed the patch, a SIW transmission line with a coupling slot on it is utilized. For inductive loading at 28 GHz, a pair of shorting pins is adopted to connect the patch to the ground while the upper metal layer of the SIW acts as the ground for the radiating patch. Another antenna fed by the same coupling slot is designed for 38 GHz band. A combined design is realized while the surface currents of the two antennas at 28 and 38 GHz maintain unchanged respectively. Measured results declare that an $S_{11} < -10$ dB bandwidth of 3.8% is achieved at 28 GHz-band while another bandwidth of 9.0% is achieved at 38 GHz-band. Since the operating principle of the antenna has no relationship with the working frequencies, design method can be extended to other frequency bands. Moreover, the proposed dual-band antenna obtains an independent tuning performance and indicates that it can be a potential candidate for forthcoming 5G mmW MIMO communication system applications.

ACKNOWLEDGMENT

The authors would like to thank Mr. T. Huo and Mr. Z. Kuai for their help with the fabrication and measurement of the antenna.

REFERENCES

[1] J. Sun, W. Shi, Z. Yang, J. Yang, and G. Gui, "Behavioral modeling and linearization of wideband RF power amplifiers using BiLSTM networks for 5G wireless systems," *IEEE Trans. Veh. Technol.*, vol. 68, no. 11, pp. 10348–10356, Nov. 2019.

[2] Z. Cao, X. Zhao, F. M. Soares, N. Tessema, and A. M. J. Koonen, "38-GHz millimeter wave beam steered fiber wireless systems for 5G indoor coverage: Architectures, devices, and links," *IEEE J. Quantum Electron.*, vol. 53, no. 1, pp. 1–9, Feb. 2017.

[3] T. S. Rappaport, S. Sun, R. Mayzus, H. Zhao, Y. Azar, K. Wang, G. N. Wong, J. K. Schulz, M. Samimi, and F. Gutierrez, "Millimeter wave mobile communications for 5G cellular: It will work!" *IEEE Access*, vol. 1, pp. 335–349, 2013.

[4] J. F. Zhang, Y. J. Cheng, Y. R. Ding, and C. X. Bai, "A dual-band shared-aperture antenna with large frequency ratio, high aperture reuse efficiency, and high channel isolation," *IEEE Trans. Antennas Propag.*, vol. 67, no. 2, pp. 853–860, Feb. 2019.

[5] C. Dehos, J. L. González, A. D. Domenico, D. Kténas, and L. Dussopt, "Millimeter-wave access and backhauling: The solution to the exponential data traffic increase in 5G mobile communications systems?" *IEEE Commun. Mag.*, vol. 52, no. 9, pp. 88–95, Sep. 2014.

[6] D. Muirhead, M. A. Imran, and K. Arshad, "Insights and approaches for low-complexity 5G small-cell base-station design for indoor dense networks," *IEEE Access*, vol. 3, pp. 1562–1572, 2015.

[7] C. Han, Y. Bi, S. Duan, and G. Lu, "Rain rate retrieval test from 25-GHz, 28-GHz, and 38-GHz millimeter-wave link measurement in beijing," *IEEE J. Sel. Topics Appl. Earth Observ. Remote Sens.*, vol. 12, no. 8, pp. 2835–2847, Aug. 2019.

[8] Y.-S. Chen, D.-J. Deng, and C.-C. Teng, "Range-based localization algorithm for next generation wireless networks using radical centers," *IEEE Access*, vol. 4, pp. 2139–2153, 2016.

[9] H. Huang, S. Guo, G. Gui, Z. Yang, J. Zhang, H. Sari, and F. Adachi, "Deep learning for physical-layer 5G wireless techniques: Opportunities, challenges and solutions," *IEEE Wireless Commun.*, to be published.

[10] C. Hansen, "WiGiG: Multi-gigabit wireless communications in the 60 GHz band," *IEEE Wireless Commun.*, vol. 18, no. 6, pp. 6–7, Dec. 2011.

[11] T. A. Levanen, J. Pirskanen, T. Koskela, J. Talvitie, and M. Valkama, "Radio interface evolution towards 5G and enhanced local area communications," *IEEE Access*, vol. 2, pp. 1005–1029, 2014.

[12] E. Hernandez-Orallo, M. Murillo-Arcila, J.-C. Cano, C. T. Calafate, J. A. Conejero, and P. Manzoni, "An analytical model based on population processes to characterize data dissemination in 5G opportunistic networks," *IEEE Access*, vol. 6, pp. 1603–1615, 2018.

[13] S. Kim, E. Visotsky, P. Moorut, K. Bechta, A. Ghosh, and C. Dietrich, "Coexistence of 5G with the incumbents in the 28 and 70 GHz bands," *IEEE J. Sel. Areas Commun.*, vol. 35, no. 6, pp. 1254–1268, Jun. 2017.

[14] T.-J. Huang, H.-T. Hsu, and H.-T. Chou, "A compact dual-band antenna at Ka-band frequencies for next generation cellular applications," in *Proc. 15th Eur. Radar Conf. (EuRAD)*, Sep. 2018, pp. 269–272.

[15] K. R. Mahmoud and A. M. Montaser, "Performance of tri-band multi-polarized array antenna for 5G mobile base station adopting polarization and directivity control," *IEEE Access*, vol. 6, pp. 8682–8694, 2018.

[16] J.-H. Lee, J.-S. Choi, and S.-C. Kim, "Cell coverage analysis of 28 GHz millimeter wave in urban microcell environment using 3-D ray tracing," *IEEE Trans. Antennas Propag.*, vol. 66, no. 3, pp. 1479–1487, Mar. 2018.

[17] B. Yang, Z. Yu, Y. Dong, J. Zhou, and W. Hong, "Compact tapered slot antenna array for 5G millimeter-wave massive MIMO systems," *IEEE Trans. Antennas Propag.*, vol. 65, no. 12, pp. 6721–6727, Dec. 2017.

[18] S. F. Jilani, Q. H. Abbasi, Z. U. Khan, T.-H. Loh, and A. Alomainy, "A Ka-band antenna based on an enhanced Franklin model for 5G cellular networks," *Microw. Opt. Technol. Lett.*, vol. 60, no. 6, pp. 1562–1566, Jun. 2018.

[19] S. F. Jilani and A. Alomainy, "A multiband millimeter-wave 2-D array based on enhanced franklin antenna for 5G wireless systems," *IEEE Antennas Wireless Propag. Lett.*, vol. 16, pp. 2983–2986, 2017.

[20] Y. Liu, S. Wang, N. Li, J.-B. Wang, and J. Zhao, "A compact dual-band dual-polarized antenna with filtering structures for sub-6 GHz base station applications," *IEEE Antennas Wireless Propag. Lett.*, vol. 17, no. 10, pp. 1764–1768, Oct. 2018.

[21] B. Feng, C. Zhu, J.-C. Cheng, C.-Y.-D. Sim, and X. Wen, "A dual-wideband dual-polarized magneto-electric dipole antenna with dual wide beamwidths for 5G MIMO microcell applications," *IEEE Access*, vol. 7, pp. 43346–43355, 2019.

[22] Z. Ren and A. Zhao, "Dual-band MIMO antenna with compact self-decoupled antenna pairs for 5G mobile applications," *IEEE Access*, vol. 7, pp. 82288–82296, 2019.

[23] D. Q. Liu, M. Zhang, H. J. Luo, H. L. Wen, and J. Wang, "Dual-band platform-free PIFA for 5G MIMO application of mobile devices," *IEEE Trans. Antennas Propag.*, vol. 66, no. 11, pp. 6328–6333, Nov. 2018.

[24] X. Liu, Y. Wu, Z. Zhuang, W. Wang, and Y. Liu, "A dual-band patch antenna for pattern diversity application," *IEEE Access*, vol. 6, pp. 51986–51993, 2018.

[25] X. Zhang and L. Zhu, "Patch antennas with loading of a pair of shorting pins toward flexible impedance matching and low cross polarization," *IEEE Trans. Antennas Propag.*, vol. 64, no. 4, pp. 1226–1233, Apr. 2016.

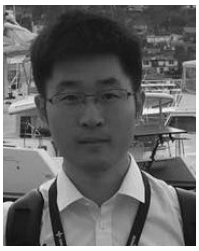

PENGFEI LIU (Student Member, IEEE) was born in Nantong, China, in 1989. He received the B.S. degree in communication engineering and the M.S. degree in electromagnetic field and microwave technology from the Harbin Institute of Technology, Harbin, China, in 2011 and 2013, respectively. He is currently pursuing the Ph.D. degree with the State Key Laboratory of Millimeter Waves, Southeast University, Nanjing, China. His research interests include RF/microwave/millimeter wave circuits and passive devices, such as antennas, antenna arrays, and filters.

XIAO-WEI ZHU (Member, IEEE) receive the M.E. and Ph.D. degrees in radio engineering from Southeast University, Nanjing, China, in 1996 and 2000, respectively.

Since 1984, he has been with Southeast University, where he is currently a Professor with the School of Information Science and Engineering. He has authored or coauthored over 90 technical publications. He holds 15 patents. His research interests include RF and antenna technologies for wireless communications, microwave and millimeter-wave theory and technology, and power amplifier (PA) nonlinear character and its linearization research, with a particular emphasis on wideband and high-efficiency GaN PAs.

Dr. Zhu was a recipient of the 1994 First-Class Science and Technology Progress Prize by the Ministry of Education of China, and the 2003 Second-Class Science and Technology Progress Prize of Jiangsu Province, China. He is a President of the Microwave Integrated Circuits and Mobile Communication Sub-Society, the Microwave Society of CIE, and the Secretary of the IEEE MTT-S/AP-S/EMC-S Joint Nanjing Chapter.

YAN ZHANG (Member, IEEE) received the B.Eng. degree in information engineering, and the Ph.D. degree in electrical engineering from Southeast University (SEU), Nanjing, China, in 2006 and 2012, respectively.

From January 2009 to July 2009, he was with the Institute for Infocomm Research (I2R), Agency for Science, Technology, and Research (A∗STAR), Singapore, as a Research Engineer. From November 2009 to December 2010, he was with the Electromagnetic Communication Laboratory, Pennsylvania State University, as a Visiting Scholar. Since December 2011, he has been a Researcher with the State Key Laboratory of Millimeter Waves, SEU. He has published over a dozens of peer-viewed articles. He holding 14 granted and filed patents. His research interests include millimeter wave and terahertz antennas, planar transmission line techniques and filters, RF and antenna design for satellite communication.

He was a recipient of the Best Student Paper Award from the 2008 International Conference on Microwave and Millimeter Wave Technology (ICMMT'2008) and 2013 International Symposium on Antennas and Propagation (ISAP'2013). He serves as a Reviewer for several journals, including the IEEE TRANSACTIONS ON ANTENNAS AND PROPAGATION, the IEEE ANTENNA AND PROPAGATION LETTERS, the IEEE MICROWAVE WIRELESS COMPONENT LETTERS, and PIER.

XIANG WANG (Student Member, IEEE) was born in Nanjing, China. He received the B.S. degree in electrical engineering from the Nanjing University of Science and Technology, Nanjing, in 2014. He is currently pursuing the Ph.D. degree in electromagnetic field and microwave technology with Southeast University, Nanjing. His current research interests include antennas, miniaturized passive circuits, oscillators, and millimeter-wave transceiver systems. He is a reviewer of several internationally journals, including *Electronics Letters*, the *International Journal of RF and Microwave Computer-Aided Engineering*, and IET *Microwaves, Antennas and Propagation*.

CHUNFENG YANG was born in Jiaxing, China, in 1994. She received the B.S. degree in communication engineering from Hangzhou Dianzi University. She is currently pursuing the M.S. degree with the State Key Laboratory of Millimeter Waves, Southeast University, Nanjing, China. Her research interests include antennas and antenna arrays.

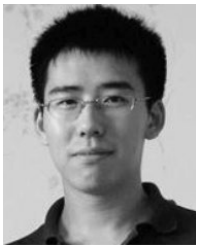

ZHI HAO JIANG (Member, IEEE) was born in Nanjing, China, in 1986. He received the B.S. degree in radio engineering from Southeast University, Nanjing, in 2008, and the Ph.D. degree in electrical engineering from Pennsylvania State University, State College, PA, USA, in 2013. From 2013 to 2016, he was a Postdoctoral Fellow with the Computational Electromagnetics and Antennas Research Laboratory, Department of Electrical Engineering, Pennsylvania State University. He is currently a Professor with the State Key Laboratory of Millimeter Waves, School of Information Science and Engineering, Southeast University. He has authored or coauthored over 90 articles in peer-reviewed international journals and conference proceedings, seven book chapters, and has four U.S. patents and a Chinese patent. He has co-edited the book *Electromagnetics of Body-Area Networks: Antennas, Propagation, and RF Systems* (Wiley/IEEE Press, 2016). His current research interests include microwave/millimeter-wave antennas and circuits, impedance surfaces, and meta-materials. He was a recipient of the Thousands of Young Talents Award by the China Government, in 2016, the Honorable Mention, in 2013, the IEEE AP-S International Symposium on Antennas and Propagation Student Paper Contest, and the 2012 A. J. Ferraro Outstanding Doctoral Research Award in electromagnetics. He also serves as a reviewer for more than 20 journals including *Nature Communications*, *Scientific Reports*, the IEEE TRANSACTIONS ON ANTENNAS AND PROPAGATION, the IEEE TRANSACTIONS ON BIOMEDICAL CIRCUITS AND SYSTEMS, the IEEE ANTENNAS AND WIRELESS PROPAGATION LETTERS, the IEEE MICROWAVE AND WIRELESS COMPONENT LETTERS, and the IEEE Antennas and Propagation Magazine.